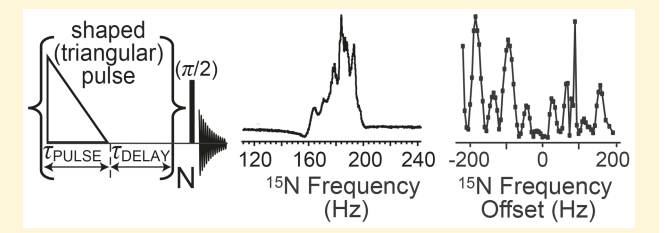


Quasi-Resonance Signal Amplification by Reversible Exchange

Thomas Theis, †, ‡ Nuwandi M. Ariyasingha, *Roman V. Shchepin, Jacob R. Lindale, ‡ Warren S. Warren. and Eduard Y. Chekmenev*, \$,10

Supporting Information

ABSTRACT: Here we present the feasibility of NMR signal amplification by reversible exchange (SABRE) using radio frequency irradiation at low magnetic field (0.05 T) in the regime where the chemical shifts of free and catalyst-bound species are similar. In SABRE, the ¹⁵N-containing substrate and parahydrogen perform simultaneous chemical exchange on an iridium hexacoordinate complex. A shaped spin-lock induced crossing (SLIC) radio frequency pulse sequence followed by a delay is applied at quasi-resonance (QUASR) conditions of ¹⁵N



spins of a 15N-enriched substrate. As a result of this pulse sequence application, 15N z-magnetization is created from the spin order of parahydrogen-derived hyperpolarized hydrides. The repetition of the pulse sequence block consisting of a shaped radio frequency pulse and the delay leads to the buildup of ¹⁵N magnetization. The modulation of this effect by the irradiation frequency, pulse duration and amplitude, delay duration, and number of pumping cycles was demonstrated. Pyridine-15N, acetonitrile $-^{15}$ N, and metronidazole $-^{15}$ N $_2$ - 13 C $_2$ substrates were studied representing three classes of compounds (five- and sixmembered heterocycles and nitrile), showing the wide applicability of the technique. Metronidazole $^{-15}N_2$ - $^{13}C_2$ is an FDAapproved antibiotic that can be injected in large quantities, promising noninvasive and accurate hypoxia sensing. The 15N hyperpolarization levels attained with QUASR-SABRE on metronidazole-15N2-13C2 were more than 2-fold greater than those with SABRE-SHEATH (SABRE in shield enables alignment transfer to heteronuclei), demonstrating that QUASR-SABRE can deliver significantly more efficient means of SABRE hyperpolarization.

onventional NMR relies on equilibrium thermal nuclear spin polarization P dictated by the Boltzmann distribution among Zeeman energy levels dependent on the applied static magnetic field B_0 . Although P can be boosted significantly by applying a stronger magnetic field (because P $\propto B_0$), P is typically on the order of $10^{-5}-10^{-6}$ for a conventional high-field NMR spectrometer (ca. 9.4 T) or MRI scanner (ca. 3 T) at room temperature, i.e., when the hightemperature approximation holds. Hyperpolarization techniques increase P to the order of unity, increasing NMR sensitivity by 4-5 orders of magnitude.

Several hyperpolarization techniques exist. 1-3 Signal amplification by reversible exchange (SABRE) is one of more recent techniques pioneered by Duckett and co-workers in 2009.⁴⁻⁷ SABRE relies on simultaneous chemical exchange of parahydrogen (p-H₂) and a to-be-hyperpolarized (HP) substrate (Figure 1a). When the transient complex is formed, the p- H_2 symmetry is broken,⁹ and the network of spin-spin couplings can enable transfer polarization from p-H2-derived hydrides to the nuclear spins of the substrate.4-7 Two major groups of

approaches have been developed for SABRE polarization transfer: the first group employs a matching static magnetic field $B_{\rm evo}$, $^{4,10-13}$ and the second group applies radio frequency (RF) pulse sequences 14,15 to approach level anticrossings (LACs) 16,17 and induce polarization transfer. Both approaches have merit depending on the application. For biomedical applications, which represent the main driver for development of hyperpolarization technology,² the key is to achieve high degrees of polarization with the long lifetimes in a suitable biomolecular motif.¹⁸ So far, approaches relying on static magnetic fields such as SABRE-SHEATH (SABRE in shield enables alignment transfer to heteronuclei) 19-21 have been the most efficient for preparation of long-lived $^{15}\mathrm{N}$ HP spin states with exponential decay constants of more than 20 min²² and P_{15N} exceeding 30%. 23,24

Received: August 29, 2018 Accepted: October 4, 2018 Published: October 4, 2018

Department of Chemistry, North Carolina State University, Raleigh, North Carolina 27695-8204, United States

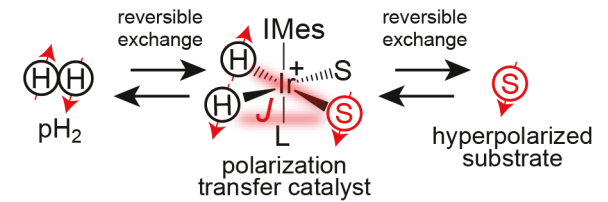
[‡]Department of Chemistry, Duke University, Durham, North Carolina 27708, United States

[§]Department of Chemistry, Integrative Biosciences (Ibio), Wayne State University, Karmanos Cancer Institute (KCI), Detroit, Michigan 48202, United States

Department of Radiology and Radiological Sciences, Vanderbilt University Institute of Imaging Science (VUIIS), Nashville, Tennessee 37232-2310, United States

[⊥]Russian Academy of Sciences, Leninskiy Prospekt 14, Moscow 119991, Russia

a Signal Amplification By Reversible Exchange (SABRE)



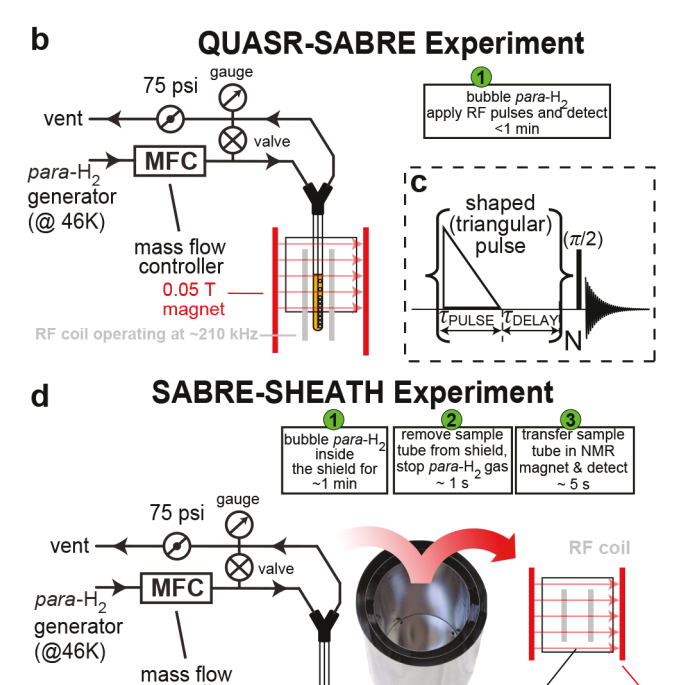


Figure 1. (a) Diagram of molecular exchange with $p\text{-H}_2$ in SABRE hyperpolarization. (b) Experimental setup for QUASR-SABRE, (c) rf pulse sequence for QUASR-SABRE, and (d) corresponding to the experimental setup for SABRE-SHEATH experiment.

three-layered

mu-metal

shield

detection

chamber

0.05 T

controller

One likely explanation as to why rf-based methods are lagging behind in the context of SABRE is the reliance on conventional high-field NMR spectrometers with small coils that only encompass a small fraction of the liquid sample in a 5 mm NMR tube that is continuously bubbled with p-H $_2$ gas. These factors result in major rf inhomogeneities. In contrast, a previous approach used in hydrogenative p-H $_2$ -induced polarization (PHIP 9,26,27), employs low-field (ca. 5–50 mT) magnets and rf excitation coils, which encompass the entire sample volume, sometimes in excess of 50 mL. Moreover, the hardware behind such low-field devices is significantly less complex and less costly compared to that of the high-field NMR spectrometers. Res. 25,33,36,37 Here it is demonstrated that these advantageous features can also be translated to SABRE.

rf-Based polarization transfer such as low-irradiation generation of high Tesla (LIGHT)-SABRE employs rf irradiation of the catalyst-bound substrate (Figure 1A), which typically has a chemical shift difference of 30-50 ppm with respect to the free substrate. Irradiation of the catalyst-bound species allows for polarization transfer from p-H₂-derived hydrides. When the complex dissociates, the p-scale p

nuclear spin polarization is preserved in the free substrate because it is not affected by the frequency-selective rf pulses. ¹⁴ Achieving this frequency-selective irradiation at high magnetic fields is trivial due to large chemical shift dispersion. For example, a 50 ppm difference is equal to \sim 2 kHz at 9.4 T. However, this difference vanishes at low magnetic fields; for example, a 50 ppm difference equals 10 Hz at 0.05 T (the magnetic field employed in this Letter), and frequency-selective rf excitation becomes challenging. We demonstrate that this challenge can be overcome through the use of quasi-resonance (QUASR) spin-lock induced crossing (SLIC) ³⁹ irradiation to polarize ¹⁵N spins from p-H₂-derived hydrides.

The QUASR-SABRE experiment (Figure 1B) is performed in a 0.05 T magnetic field using a previously described $p\text{-H}_2$ bubbling setup in a medium-walled 5 mm NMR tube. 25,40,41 During $p\text{-H}_2$ bubbling, a triangular-shaped pulse is applied for a duration of τ_{PULSE} followed by a delay period of τ_{DELAY} . The process is repeated, and the net z-magnetization increases during this "rf pumping" process. The resulting magnetization can be conveniently assessed by applying a broad-band excitation ($\pi/2$) rf pulse, Figure 1c. We compare the performance of this QUASR-SABRE approach with the SABRE-SHEATH approach (Figure 1d), which has been employed previously to obtain record-high 15 N polarization in excess of 30%. 23,24

The previously described SABRE-SHEATH setup, 40,41 15N rf coil, and 0.05 T magnet have been employed here. ⁴² Samples of three substrates and the IrIMes catalyst precursor in perdeuterated methanol were prepared as follows: pyridi $ne^{-15}N/catalyst$, ~20 mM/~1 mM; acetonitrile $-^{15}N/catalyst$, \sim 40 mM/ \sim 1-2 mM; metronidazole- $^{15}N_2$ - $^{13}C_2$ /catalyst, ~20 mM/~1 mM. All 15N-enriched compounds were purchased from Isotec. The rf pulse sequence was coded and applied on a Kea-2 NMR spectrometer (Magritek, New Zealand) using a Tomco rf amplifier. The employed Kea-2 spectrometer was operated in the signal averaging mode, where the signal was averaged during the multiscan acquisition version being added. As a result, the signal integral value from the multiscan spectrum is similar to that acquired using onescan acquisition, e.g., the integral values of spectra shown in corresponding displays in Figures 2-4 can be compared directly without any scaling even though the spectra were recorded using different numbers of scans. A three-layered mumetal magnetic shield was employed (Magnetic Shield Corp., Bensenville, IL, P/N ZG-206). All data were acquired employing 75-80% p-H₂ gas prepared using a home-built p-H₂ generator based on a Sunpower cryochiller at a flow rate of 150 standard cubic centimeters per minute (sccm). For the SABRE experiments, the following conditions were used: 75 psi back-pressure and 70 sccm p-H₂ flow rate (Figure 1b,d). The flow rate was maintained by a mass flow controller (MFC, Sierra Instruments, Monterey, CA, P/N C100L-DD-OV1-SV1-PV2-V1-S0-C0).

Low-field detection of HP compounds offers sufficient detection sensitivity in the context of NMR detection of HP states. However, detection of thermal polarization is challenging due to low P even at high concentrations (see the Supporting Information (SI) for details). As a result, the quantification of 15 N enhancements ($\varepsilon_{15\rm N}$) and polarization ($P_{15\rm N}$) relied on signal-to-noise measurements (see the SI for details) in order to determine the minimum values achieved.

¹⁵N NMR spectra with a high signal-to-noise ratio were obtained for all three studied molecules pyridine-¹⁵N,

The Journal of Physical Chemistry Letters

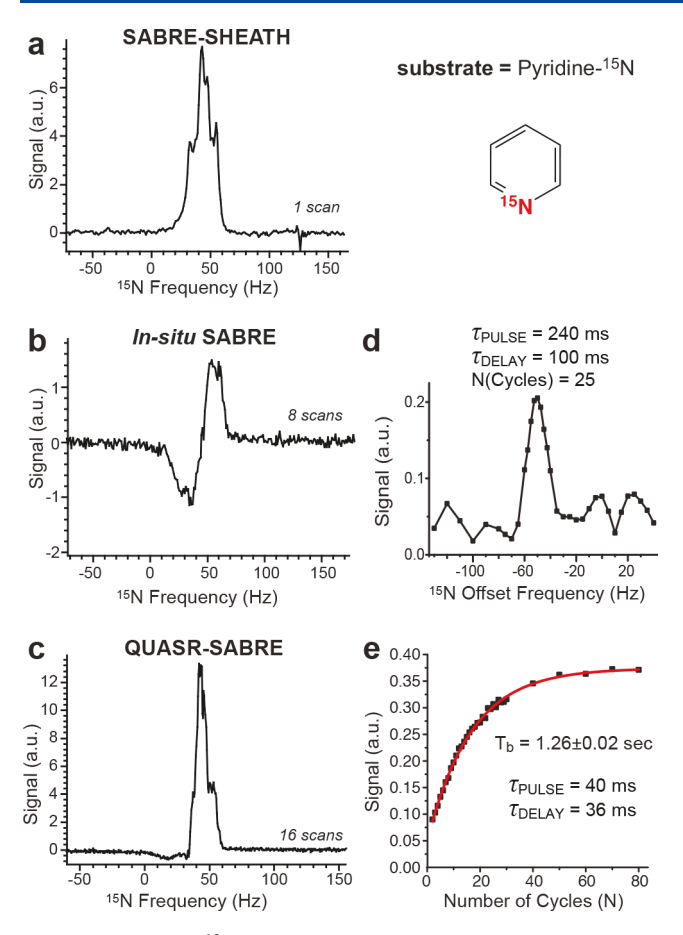


Figure 2. Pyridine—¹⁵N data. The other experimental conditions were as follows: 20 mM pyridine—¹⁵N, 1 mM catalyst in CD₃OD. Note the width of the signal in panels (b) and (d). (a) ¹⁵N spectrum obtained after performing SABRE-SHEATH; (b) ¹⁵N spectrum recorded using a 90° excitation pulse when bubbling *p*-H₂ in situ with the 0.05 T magnet; (c) ¹⁵N spectrum obtained after performing QUASR-SABRE; (d) ¹⁵N QUASR-SABRE signal dependence on the applied rf offset from the actual resonance condition; (e) buildup of the ¹⁵N QUASR-SABRE signal as a function of the number of pumping cycles. Note that the individual spectra employed for figures in panels (d) and (e) were autophased, and the data is presented in the magnitude mode.

acetonitrile $^{-15}$ N, and metronidazole $^{-15}$ N $_2$ - 13 C $_2$ using SABRE-SHEATH (Figures 2a, 3a, and 4a, respectively) and QUASR-SABRE (Figures 2c, 3c, and 4c, respectively). We note that while p-H $_2$ bubbling through the sample placed in 0.05 T leads to a 15 N signal even without rf pulses (Figures 2b, 3b, and 4b, respectively), this 15 N signal is distinctly antiphase 14,42,44 and has significantly lower intensity compared to those obtained using SABRE-SHEATH and QUASR-SABRE protocols.

The key distinct feature of the QUASR-SABRE phenomenon is a strong rf offset frequency dependence; Figures 2d and 4d demonstrate the dependence of the 15 N QUASR-SABRE signal for pyridine— 15 N and metronidazole— 15 N₂— 13 C₂, respectively. Note that very small signal is obtained at the resonance frequency. The maximum intensity of 15 N QUASR-SABRE was compared to that of SABRE-SHEATH and is reported here as the ratio of the 15 N QUASR-SABRE and SABRE-SHEATH signals, η . We find an η of ~1.0 for pyridine— 15 N, η of ~0.44 for acetonitrile— 15 N, and η of (at least) ~2.4 for metronidazole— 15 N₂— 13 C₂. The relatively low η

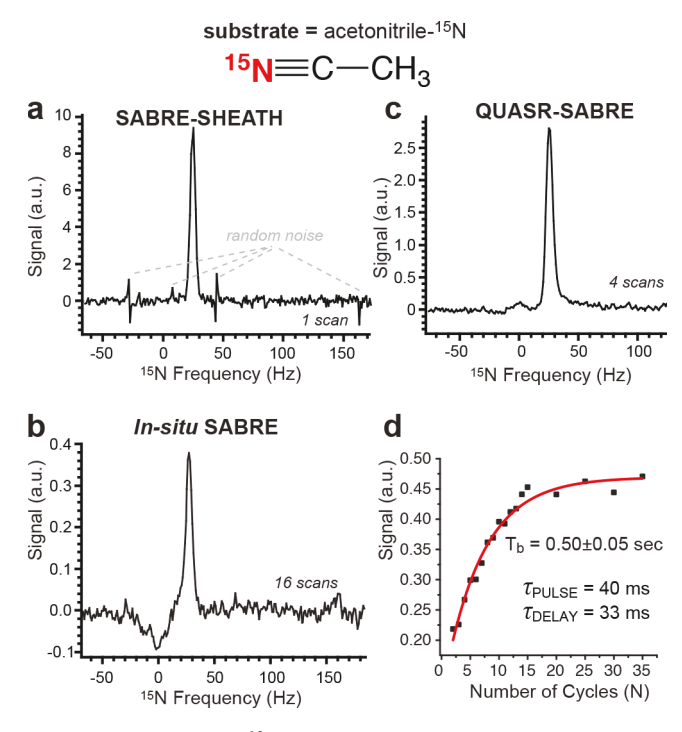


Figure 3. Acetonitrile— 15 N data. The other experimental conditions were as follows: 40 mM acetonitrile— 15 N, 1 or 2 mM catalyst in CD₃OD. Note that the width of the signal in panels (a) and (c) is nearly the same as that opposed to pyridine— 15 N case. (a) 15 N spectrum obtained after performing SABRE-SHEATH; (b) 15 N spectrum recorded using a 90° excitation pulse when bubbling $p\text{-H}_2$ in situ with the 0.05 T magnet; (c) 15 N spectrum obtained after performing QUASR-SABRE; (d) buildup of the 15 N QUASR-SABRE signal as a function of the number of pumping cycles. Note that the individual spectra employed for figures in panel (d) were autophased, and the data are presented in the magnitude mode.

value for acetonitrile-15N is in part explained by the fact that frequency optimization was not performed, and the data were recorded using the frequency offset parameter optimized for pyridine-15N, which unfortunately did not provide a fair comparison. On the basis of the range of the frequency optimization data for pyridine-15N (Figure 2e) and for metronidazole $-{}^{15}N_2-{}^{13}C_2$ (Figure4d), we estimate that this optimization may potentially yield an improvement of up to 10-fold. We note that the η value for metronidazole-15N2-13C2 assumes that both 15N sites are HP via SABRE-SHEATH and QUASR-SABRE protocols. While SABRE-SHEATH indeed yields hyperpolarization of both ¹⁵N sites due to spin-relay of polarization at very low magnetic fields (the Earth's field (ca. 50 μ T) and below), QUASR-SABRE may yield hyperpolarization of only one (N₃) site, Figure 4. If that is the case, then η would be effectively doubled to 4.8 because only one ¹⁵N site contributes to the QUASR-SABRE signal (Figure 4c) versus two ¹⁵N sites to the SABRE-SHEATH NMR signal (Figure 4a). We note that the full width at the half-height (FWHH) of the NMR spectral line was approximately the same for SABRE-SHEATH and QUASR-SABRE NMR spectra for acetonitrile-15N and metronidazo $le^{-15}N_2-^{13}C_2$ (Figures 3 and 4, respectively), whereas the QUASR-SABRE spectral line FWHH was approximately half of that for the SABRE-SHEATH spectrum for pyridine-15N (Figure 2 panels (c) and (a), respectively). The latter observation may in part explain the pyridine- 15 N η value,

The Journal of Physical Chemistry Letters

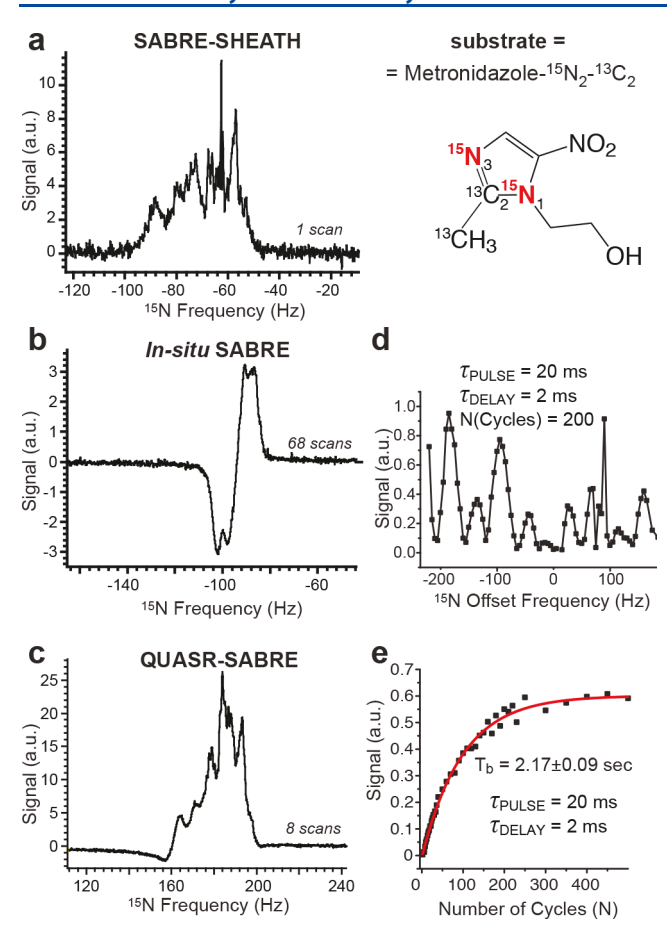


Figure 4. Metronidazole $^{-15}$ N $_2$ - 13 C $_2$ data. The other experimental conditions were as follows: ~20 mM metronidazole $^{-15}$ N $_2$ - 13 C $_2$, 1 or 2 mM catalyst in CD $_3$ OD. Note that the width of the signal in panels (a) and (c) is nearly the same as that opposed to the pyridine $^{-15}$ N case. (a) 15 N spectrum obtained after performing SABRE-SHEATH; (b) 15 N spectrum recorded using a 90° excitation pulse when bubbling p-H $_2$ in situ with the 0.05 T magnet; (c) 15 N spectrum obtained after performing QUASR-SABRE; (d) 15 N QUASR-SABRE signal dependence on the frequency of the applied rf-shaped pulse; (e) buildup of the 15 N QUASR-SABRE signal as a function of the number of pumping cycles N. Note that the individual spectra employed for figures in panels (d) and (e) were autophased, and the data are presented in the magnitude mode.

which is significantly lower than that of metronidazo- $le^{-15}N_2-^{13}C_2$.

All three molecules studied exhibited a clear and strong dependence of the ¹⁵N QUASR-SABRE signal on the duration of the pulse (τ_{PULSE}) and the duration of the delay (τ_{DELAY}) (Figures S2a, S3a, and S3b and Figures S4a, S2b, S3c, and S4b, respectively. This strong dependence is likely due to the dynamics and kinetics of the substrate and p-H2 exchange on the catalyst. When the au_{PULSE} and au_{DELAY} are in sync with chemistry of exchange, the maximum QUASR-SABRE signal may be achieved. However, we note that the QUASR-SABRE signal has very complex dependence on τ_{PULSE} and τ_{DELAY} . For example, the τ_{PULSE} curves for acetonitrile-15N are vastly different at $\tau_{\rm DELAY}$ of 2 ms (Figure S3a) and $\tau_{\rm DELAY}$ of 33 ms (Figure S3b). Future theoretical work is certainly warranted to study this complex behavior of the QUASR-SABRE effect, which is outside of the scope of this first phenomenological report.

The second key feature of the QUASR-SABRE effect allows for continuous rf pumping of $^{15}{\rm N}$ z-magnetization: Figures 2e, 3d, and 4e for the three studied compounds, respectively. The fitting of the exponential dependence of the buildup process yielded $T_{\rm b}$ of 0.5 \pm 0.05 s for acetonitrile– $^{15}{\rm N}$, $T_{\rm b}$ of 1.26 \pm 0.02 s for pyridine– $^{15}{\rm N}$, and $T_{\rm b}$ of 2.17 \pm 0.09 s for metronidazole– $^{15}{\rm N}_2$ – $^{13}{\rm C}_2$. The $T_{\rm b}$ values correlate well with η values with R^2 of 0.93 (Figure 5), suggesting that the buildup

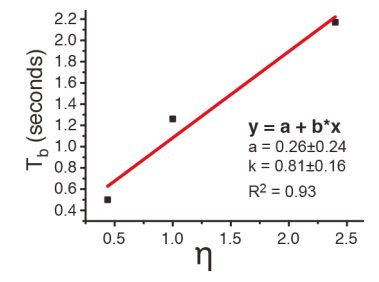


Figure 5. Correlation plot of $T_{\rm b}$ and η for the three studied compounds.

rate may be affecting the efficiency of the QUASR-SABRE polarization process. A likely explanation of this observation is the contribution of the polarization destruction processes to $T_{\rm b}$ as follows: when the destruction due to rf pulses is significant, $T_{\rm b}$ is effectively reduced, resulting in lower ¹⁵N signals in a manner analogous to that of batch-mode spin exchange optical pumping (SEOP). Further experimental and theoretical studies are certainly warranted in the future to maximize the efficiency of the QUASR-SABRE approach described here.

All experiments were performed at room temperature (ca. 298 K). We note that the rf pumping of the QUASR-SABRE process needs to be effectively matched to the chemical exchange dynamics in order to maximize the polarization transfer efficiency to yield the highest P_{15N} value. Therefore, it is expected that the optimal values of au_{PULSE} and au_{DELAY} (Figures S2-S4) would exhibit temperature dependence, because temperature modulates the rates of substrate and p-H₂ exchange. Moreover, it is possible that the optimum temperature (i.e., yielding the highest value of $P_{15\mathrm{N}}$) may be significantly different from room temperature and may be different from the optimal temperature of the SABRE-SHEATH process (note that the optimal SABRE-SHEATH temperature for pyridine-15N and for metronidazole-15N2-13C2 corresponds to approximately room temperature, i.e., SABRE-SHEATH experiments were optimized with respect to temperature). As a result, some additional improvement in the maximum value of P_{15N} may be potentially expected for the QUASR-SABRE process.

We have also investigated the dependence of the QUASR-SABRE signal on the amplitude of the SLIC power amplitude. Figure S4c exhibits a plateau (with a range of approximately 6 dB) with relatively steep slopes on both sides. This trend is expected because LAC conditions are usually created in a relatively narrow power range. 16,49

Optimization of $P_{15\rm N}$ was not the goal of this Letter. Moreover, due to lack of direct $^{15}\rm N$ signal reference (due to the insufficient thermal equilibrium signal), we can only report the lower limits of $\varepsilon_{15\rm N}$ and $P_{15\rm N}$ values. Metronidazole– $^{15}\rm N$ – $^{13}\rm C_2$ QUASR-SABRE estimates were $\varepsilon_{15\rm N}\approx 9\times 10^5$ and $P_{15\rm N}\approx 1.5\%$ (these values are doubled if only the $\rm N_3$ site is HP).

Metronidazole $^{-15}$ N $_2$ $^{-13}$ C $_2$ SABRE-SHEATH estimates were $\varepsilon_{15\mathrm{N}}\approx 3.7\times 10^5$ and $P_{15\mathrm{N}}\approx 0.6\%$. Note that these lower-limit estimates are in good agreement with $P_{15\mathrm{N}}\approx 1.5\%$ reported for SABRE-SHEATH under similar conditions using detection provided by a high-resolution 9.4 T NMR spectrometer. 40,41 Pyridine $^{-15}$ N lower-limit estimates were $\varepsilon_{15\mathrm{N}}\approx 6.6\times 10^5$ and $P_{15\mathrm{N}}\approx 1.1\%$ for both QUASR-SABRE and SABRE-SHEATH, in line with previous SABRE-SHEATH studies. 19,20 Acetonitrile $^{-15}$ N lower-limit estimates were $\varepsilon_{15\mathrm{N}}\approx 5.3\times 10^4$ and $P_{15\mathrm{N}}\approx 0.09\%$ for QUASR-SABRE and $\varepsilon_{15\mathrm{N}}\approx 1.2\times 10^5$ and $P_{15\mathrm{N}}\approx 0.2\%$ for SABRE-SHEATH, respectively. See the SI for details.

With regards to the limitations of the QUASR-SABRE method, it remains to be seen if QUASR-SABRE is capable of hyperpolarization of long-range spin sites in the substrate compounds. Moreover, future systematic experimental and theoretical studies are certainly needed to further optimize the efficiency of the QUASR-SABRE technique. For example, more advanced shaped forms (e.g., sine, exponential, trapezoid, etc.) and strategies (adiabatic pulses) can be envisioned.

In summary, an rf-based polarization transfer approach has been presented for hyperpolarization of ¹⁵N sites. At least in some compounds, this method appears to be more efficient than the SABRE-SHEATH approach, which has already been shown to yield more than 30% ¹⁵N polarization. ²⁴ This is remarkable because in all previous demonstrations of rf-SABRE approaches yielded significantly lower polarization than static field matching/field cycling approaches. We hope that QUASR-SABRE may ultimately yield 15N polarization of the order of unity for a wide range of biomolecules. The employed pulse sequence is a shaped variant of the SLIC pulse sequence,³⁹ which has the benefit of using low power levels. The applicability of this technique has been explored for three different types of compounds (six- and five-membered Nheterocycles and acetonitrile), including the antibiotic metronidazole. Metronidazole is an antibiotic that can be administered in large $doses^{50}$ and contains the nitroimidazole moiety, which has been exploited in a wide range of molecular contrast agents for hypoxia sensing using positron emission tomography (PET). 51-56 Therefore, metronidazole is a promising candidate as a molecular probe for hypoxia imaging using HP MRI.41

ASSOCIATED CONTENT

S Supporting Information

The Supporting Information is available free of charge on the ACS Publications website at DOI: 10.1021/acs.jp-clett.8b02669.

Computation of ¹⁵N signal enhancement and polarization values, photograph of the shaped rf pulse detected by the oscilloscope, and figures of the QUASR-SABRE effect (PDF)

AUTHOR INFORMATION

Corresponding Author

*E-mail: chekmenev@wayne.edu.

ORCID 6

Thomas Theis: 0000-0001-6779-9978

Eduard Y. Chekmenev: 0000-0002-8745-8801

Fundina

This work was supported by NSF under Grants CHE-1058727, CHE-1363008, CHE-1416268, and CHE-1836308. Research reported in this publication was also supported by the National

Institute of Biomedical Imaging and Bioengineering of the NIH under R21EB025313 and 1R21EB020323, by that National Cancer Institute under 1R21CA220137, and by DOD CDMRP under BRP W81XWH-12-1-0159/BC112431 and W81XWH-15-1-0271.

Notes

The authors declare no competing financial interest.

REFERENCES

- (1) Goodson, B. M.; Whiting, N.; Coffey, A. M.; Nikolaou, P.; Shi, F.; Gust, B. M.; Gemeinhardt, M. E.; Shchepin, R. V.; Skinner, J. G.; Birchall, J. R.; et al. Hyperpolarization Methods for MRS. *Emagres* **2015**, *4*, 797–810.
- (2) Nikolaou, P.; Goodson, B. M.; Chekmenev, E. Y. NMR Hyperpolarization Techniques for Biomedicine. *Chem. Eur. J.* **2015**, 21, 3156–3166.
- (3) Kovtunov, K. V.; Pokochueva, E.; Salnikov, O. G.; Cousin, S.; Kurzbach, D.; Vuichoud, B.; Jannin, S.; Chekmenev, E. Y.; Goodson, B. M.; Barskiy, D. A.; et al. Hyperpolarized NMR: D-DNP, PHIP, and SABRE. *Chem. Asian J.* **2018**, *13*, 1857–1871.
- (4) Adams, R. W.; Aguilar, J. A.; Atkinson, K. D.; Cowley, M. J.; Elliott, P. I. P.; Duckett, S. B.; Green, G. G. R.; Khazal, I. G.; Lopez-Serrano, J.; Williamson, D. C. Reversible Interactions with Para-Hydrogen Enhance NMR Sensitivity by Polarization Transfer. *Science* **2009**, *323*, 1708–1711.
- (5) Adams, R. W.; Duckett, S. B.; Green, R. A.; Williamson, D. C.; Green, G. G. R. A Theoretical Basis for Spontaneous Polarization Transfer in Non-Hydrogenative Parahydrogen-Induced Polarization. *J. Chem. Phys.* **2009**, *131*, 194505.
- (6) Atkinson, K. D.; Cowley, M. J.; Duckett, S. B.; Elliott, P. I. P.; Green, G. G. R.; López-Serrano, J.; Khazal, I. G.; Whitwood, A. C. Para-Hydrogen Induced Polarization without Incorporation of Para-Hydrogen into the Analyte. *Inorg. Chem.* **2009**, *48*, 663–670.
- (7) Atkinson, K. D.; Cowley, M. J.; Elliott, P. I. P.; Duckett, S. B.; Green, G. G. R.; Lopez-Serrano, J.; Whitwood, A. C. Spontaneous Transfer of Parahydrogen Derived Spin Order to Pyridine at Low Magnetic Field. *J. Am. Chem. Soc.* **2009**, *131*, 13362–13368.
- (8) Rayner, P. J.; Duckett, S. B. Signal Amplification by Reversible Exchange (SABRE): From Discovery to Diagnosis. *Angew. Chem., Int. Ed.* **2018**, *57*, 6742–6753.
- (9) Bowers, C. R.; Weitekamp, D. P. Transformation of Symmetrization Order to Nuclear-Spin Magnetization by Chemical-Reaction and Nuclear-Magnetic-Resonance. *Phys. Rev. Lett.* **1986**, *57*, 2645–2648.
- (10) Shchepin, R. V.; Truong, M. L.; Theis, T.; Coffey, A. M.; Shi, F.; Waddell, K. W.; Warren, W. S.; Goodson, B. M.; Chekmenev, E. Y. Hyperpolarization of "Neat" Liquids by NMR Signal Amplification by Reversible Exchange. *J. Phys. Chem. Lett.* **2015**, *6*, 1961–1967.
- (11) Green, R. A.; Adams, R. W.; Duckett, S. B.; Mewis, R. E.; Williamson, D. C.; Green, G. G. R. The Theory and Practice of Hyperpolarization in Magnetic Resonance Using Parahydrogen. *Prog. Nucl. Magn. Reson. Spectrosc.* **2012**, *67*, 1–48.
- (12) Hövener, J. B.; Schwaderlapp, N.; Lickert, T.; Duckett, S. B.; Mewis, R. E.; Highton, L. A. R.; Kenny, S. M.; Green, G. G. R.; Leibfritz, D.; Korvink, J. G.; et al. A Hyperpolarized Equilibrium for Magnetic Resonance. *Nat. Commun.* **2013**, *4*, 2946.
- (13) Barskiy, D. A.; Kovtunov, K. V.; Koptyug, I. V.; He, P.; Groome, K. A.; Best, Q. A.; Shi, F.; Goodson, B. M.; Shchepin, R. V.; Truong, M. L.; et al. In Situ and Ex Situ Low-Field NMR Spectroscopy and MRI Endowed by SABRE Hyperpolarization. *ChemPhysChem* **2014**, *15*, 4100–4107.
- (14) Theis, T.; Truong, M.; Coffey, A. M.; Chekmenev, E. Y.; Warren, W. S. LIGHT-SABRE Enables Efficient in-Magnet Catalytic Hyperpolarization. *J. Magn. Reson.* **2014**, 248, 23–26.
- (15) Pravdivtsev, A. N. SABRE Hyperpolarization of Bipyridine Stabilized Ir-Complex at High, Low and Ultralow Magnetic Fields. *Z. Phys. Chem.* **2017**, 231, 497–511.

- (16) Pravdivtsev, A. N.; Yurkovskaya, A. V.; Zimmermann, H.; Vieth, H.-M.; Ivanov, K. L. Transfer of SABRE-Derived Hyperpolarization to Spin-1/2 Heteronuclei. *RSC Adv.* **2015**, *5*, 63615–63623
- (17) Ivanov, K. L.; Pravdivtsev, A. N.; Yurkovskaya, A. V.; Vieth, H.-M.; Kaptein, R. The Role of Level Anti-Crossings in Nuclear Spin Hyperpolarization. *Prog. Nucl. Magn. Reson. Spectrosc.* **2014**, *81*, 1–36.
- (18) Hövener, J.-B.; Pravdivtsev, A. N.; Kidd, B.; Bowers, C. R.; Glöggler, S.; Kovtunov, K. V.; Plaumann, M.; Katz-Brull, R.; Buckenmaier, K.; Jerschow, A.; et al. Parahydrogen-Based Hyperpolarization for Biomedicine. *Angew. Chem., Int. Ed.* **2018**, *57*, 11140–11162.
- (19) Theis, T.; Truong, M. L.; Coffey, A. M.; Shchepin, R. V.; Waddell, K. W.; Shi, F.; Goodson, B. M.; Warren, W. S.; Chekmenev, E. Y. Microtesla SABRE Enables 10% Nitrogen-15 Nuclear Spin Polarization. J. Am. Chem. Soc. 2015, 137, 1404—1407.
- (20) Truong, M. L.; Theis, T.; Coffey, A. M.; Shchepin, R. V.; Waddell, K. W.; Shi, F.; Goodson, B. M.; Warren, W. S.; Chekmenev, E. Y. ¹⁵N Hyperpolarization by Reversible Exchange Using SABRE-SHEATH. *J. Phys. Chem. C* **2015**, *119*, 8786–8797.
- (21) Colell, J. F. P.; Logan, A. W. J.; Zhou, Z.; Shchepin, R. V.; Barskiy, D. A.; Ortiz, G. X.; Wang, Q.; Malcolmson, S. J.; Chekmenev, E. Y.; Warren, W. S.; et al. Generalizing, Extending, and Maximizing Nitrogen-15 Hyperpolarization Induced by Parahydrogen in Reversible Exchange. *J. Phys. Chem. C* 2017, 121, 6626–6634.
- (22) Theis, T.; Ortiz, G. X.; Logan, A. W. J.; Claytor, K. E.; Feng, Y.; Huhn, W. P.; Blum, V.; Malcolmson, S. J.; Chekmenev, E. Y.; Wang, Q.; et al. Direct and Cost-Efficient Hyperpolarization of Long-Lived Nuclear Spin States on Universal ¹⁵N₂-Diazirine Molecular Tags. *Sci. Adv.* **2016**, *2*, e1501438.
- (23) Barskiy, D. A.; Shchepin, R. V.; Coffey, A. M.; Theis, T.; Warren, W. S.; Goodson, B. M.; Chekmenev, E. Y. Over 20% ¹⁵N Hyperpolarization in under One Minute for Metronidazole, an Antibiotic and Hypoxia Probe. *J. Am. Chem. Soc.* **2016**, *138*, 8080–8083.
- (24) Kidd, B. E.; Gesiorski, J. L.; Gemeinhardt, M. E.; Shchepin, R. V.; Kovtunov, K. V.; Koptyug, I. V.; Chekmenev, E. Y.; Goodson, B. M. Facile Removal of Homogeneous SABRE Catalysts for Purifying Hyperpolarized Metronidazole, a Potential Hypoxia Sensor. *J. Phys. Chem. C* 2018, 122, 16848–16852.
- (25) Truong, M. L.; Shi, F.; He, P.; Yuan, B.; Plunkett, K. N.; Coffey, A. M.; Shchepin, R. V.; Barskiy, D. A.; Kovtunov, K. V.; Koptyug, I. V.; et al. Irreversible Catalyst Activation Enables Hyperpolarization and Water Solubility for NMR Signal Amplification by Reversible Exchange. J. Phys. Chem. B 2014, 118, 13882–13889.
- (26) Bowers, C. R.; Weitekamp, D. P. Para-Hydrogen and Synthesis Allow Dramatically Enhanced Nuclear Alignment. *J. Am. Chem. Soc.* **1987**, *109*, 5541–5542.
- (27) Eisenschmid, T. C.; Kirss, R. U.; Deutsch, P. P.; Hommeltoft, S. I.; Eisenberg, R.; Bargon, J.; Lawler, R. G.; Balch, A. L. Para Hydrogen Induced Polarization in Hydrogenation Reactions. *J. Am. Chem. Soc.* **1987**, *109*, 8089–8091.
- (28) Waddell, K. W.; Coffey, A. M.; Chekmenev, E. Y. In Situ Detection of PHIP at 48 mT: Demonstration Using a Centrally Controlled Polarizer. J. Am. Chem. Soc. 2011, 133, 97–101.
- (29) Coffey, A. M.; Shchepin, R. V.; Wilkens, K.; Waddell, K. W.; Chekmenev, E. Y. A Large Volume Double Channel ¹H-X RF Probe for Hyperpolarized Magnetic Resonance at 0.0475 T. *J. Magn. Reson.* **2012**, 220, 94–101.
- (30) Kovtunov, K. V.; Truong, M. L.; Barskiy, D. A.; Koptyug, I. V.; Coffey, A. M.; Waddell, K. W.; Chekmenev, E. Y. Long-Lived Spin States for Low-Field Hyperpolarized Gas MRI. *Chem. Eur. J.* **2014**, 20, 14629–14632.
- (31) Kovtunov, K. V.; Truong, M. L.; Barskiy, D. A.; Salnikov, O. G.; Bukhtiyarov, V. I.; Coffey, A. M.; Waddell, K. W.; Koptyug, I. V.; Chekmenev, E. Y. Propane-D₆ Heterogeneously Hyperpolarized by Parahydrogen. *J. Phys. Chem. C* **2014**, *118*, 28234–28243.
- (32) Coffey, A. M.; Shchepin, R. V.; Truong, M. L.; Wilkens, K.; Pham, W.; Chekmenev, E. Y. Open-Source Automated Parahydrogen

- Hyperpolarizer for Molecular Imaging Using ¹³C Metabolic Contrast Agents. *Anal. Chem.* **2016**, *88*, 8279–8288.
- (33) Coffey, A. M.; Shchepin, R. V.; Feng, B.; Colon, R. D.; Wilkens, K.; Waddell, K. W.; Chekmenev, E. Y. A Pulse Programmable Parahydrogen Polarizer Using a Tunable Electromagnet and Dual Channel NMR Spectrometer. J. Magn. Reson. 2017, 284, 115–124.
- (34) Hövener, J.-B.; Chekmenev, E. Y.; Harris, K. C.; Perman, W.; Robertson, L.; Ross, B. D.; Bhattacharya, P. PASADENA Hyperpolarization of ¹³C Biomolecules: Equipment Design and Installation. *MAGMA* **2009**, 22, 111–121.
- (35) Hövener, J.-B.; Chekmenev, E. Y.; Harris, K. C.; Perman, W.; Tran, T.; Ross, B. D.; Bhattacharya, P. Quality Assurance of PASADENA Hyperpolarization for ¹³C Biomolecules. *MAGMA* **2009**, *22*, 123–134.
- (36) Kadlecek, S.; Vahdat, V.; Nakayama, T.; Ng, D.; Emami, K.; Rizi, R. A Simple and Low-Cost Device for Generating Hyperpolarized Contrast Agents Using Parahydrogen. *NMR Biomed.* **2011**, 24, 933–942.
- (37) Borowiak, R.; Schwaderlapp, N.; Huethe, F.; Lickert, T.; Fischer, E.; Bär, S.; Hennig, J.; von Elverfeldt, D.; Hövener, J.-B. A Battery-Driven, Low-Field NMR Unit for Thermally and Hyperpolarized Samples. *MAGMA* **2013**, *26*, 491–499.
- (38) Pravdivtsev, A. N.; Yurkovskaya, A. V.; Zimmermann, H.; Vieth, H.-M.; Ivanov, K. L. Enhancing NMR of Insensitive Nuclei by Transfer of SABRE Spin Hyperpolarization. *Chem. Phys. Lett.* **2016**, 661, 77–82.
- (39) DeVience, S. J.; Walsworth, R. L.; Rosen, M. S. Preparation of Nuclear Spin Singlet States Using Spin-Lock Induced Crossing. *Phys. Rev. Lett.* **2013**, *111*, 5.
- (40) Shchepin, R. V.; Jaigirdar, L.; Theis, T.; Warren, W. S.; Goodson, B. M.; Chekmenev, E. Y. Spin Relays Enable Efficient Long-Range Heteronuclear Signal Amplification by Reversible Exchange. *J. Phys. Chem. C* **2017**, *121*, 28425–28434.
- (41) Shchepin, R. V.; Jaigirdar, L.; Chekmenev, E. Y. Spin-Lattice Relaxation of Hyperpolarized Metronidazole in Signal Amplification by Reversible Exchange in Micro-Tesla Fields. *J. Phys. Chem. C* **2018**, 122, 4984–4996.
- (42) Shchepin, R. V.; Barskiy, D. A.; Coffey, A. M.; Feldman, M. A.; Kovtunova, L. M.; Bukhtiyarov, V. I.; Kovtunov, K. V.; Goodson, B. M.; Koptyug, I. V.; Chekmenev, E. Y. Robust Imidazole- $^{15}\mathrm{N}_2$ Synthesis for High-Resolution Low-Field (0.05 T) $^{15}\mathrm{N}$ hyperpolarized NMR Spectroscopy. *ChemistrySelect* **2017**, *2*, 4478–4483.
- (43) Coffey, A. M.; Truong, M. L.; Chekmenev, E. Y. Low-Field MRI Can Be More Sensitive Than High-Field MRI. *J. Magn. Reson.* **2013**, 237, 169–174.
- (44) Kovtunov, K. V.; Kidd, B. E.; Salnikov, O. G.; Bales, L. B.; Gemeinhardt, M. E.; Gesiorski, J.; Shchepin, R. V.; Chekmenev, E. Y.; Goodson, B. M.; Koptyug, I. V. Imaging of Biomolecular NMR Signals Amplified by Reversible Exchange with Parahydrogen inside an MRI Scanner. *J. Phys. Chem. C* 2017, 121, 25994—25999.
- (45) Walker, T. G. Fundamentals of Spin-Exchange Optical Pumping. *Journal of Physics: Conference Series* **2011**, 294, 012001.
- (46) Nikolaou, P.; Coffey, A. M.; Ranta, K.; Walkup, L. L.; Gust, B.; Barlow, M. J.; Rosen, M. S.; Goodson, B. M.; Chekmenev, E. Y. Multi-Dimensional Mapping of Spin-Exchange Optical Pumping in Clinical-Scale Batch-Mode ¹²⁹Xe Hyperpolarizers. *J. Phys. Chem. B* **2014**, *118*, 4809–4816.
- (47) Nikolaou, P.; Coffey, A. M.; Walkup, L. L.; Gust, B. M.; Whiting, N.; Newton, H.; Barcus, S.; Muradyan, I.; Dabaghyan, M.; Moroz, G. D.; et al. Near-Unity Nuclear Polarization with an 'Open-Source' ¹²⁹Xe Hyperpolarizer for NMR and MRI. *Proc. Natl. Acad. Sci. U. S. A.* **2013**, *110*, 14150–14155.
- (48) Barskiy, D. A.; Coffey, A. M.; Nikolaou, P.; Mikhaylov, D. M.; Goodson, B. M.; Branca, R. T.; Lu, G. J.; Shapiro, M. G.; Telkki, V.-V.; Zhivonitko, V. V.; et al. NMR Hyperpolarization Techniques of Gases. *Chem. Eur. J.* **2017**, 23, 725–751.
- (49) Barskiy, D. A.; Salnikov, O. G.; Romanov, A. S.; Feldman, M. A.; Coffey, A. M.; Kovtunov, K. V.; Koptyug, I. V.; Chekmenev, E. Y. NMR Spin-Lock Induced Crossing (SLIC) Dispersion and Long-

- Lived Spin States of Gaseous Propane at Low Magnetic Field (0.05 T). J. Magn. Reson. 2017, 276, 78-85.
- (50) Erickson, S. H.; Oppenheim, G. L.; Smith, G. H. Metronidazole in Breast Milk. Obstet. Gynecol. 1981, 57, 48-50.
- (51) Kizaka-Kondoh, S.; Konse-Nagasawa, H. Significance of Nitroimidazole Compounds and Hypoxia-Inducible Factor-1 for Imaging Tumor Hypoxia. *Cancer Sci.* **2009**, *100*, 1366–1373.
- (52) Procissi, D.; Claus, F.; Burgman, P.; Koziorowski, J.; Chapman, J. D.; Thakur, S. B.; Matei, C.; Ling, C. C.; Koutcher, J. A. In Vivo ¹⁹F Magnetic Resonance Spectroscopy and Chemical Shift Imaging of Tri-Fluoro-Nitroimidazole as a Potential Hypoxia Reporter in Solid Tumors. *Clin. Cancer Res.* **2007**, *13*, 3738–3747.
- (53) Komar, G.; Seppänen, M.; Eskola, O.; Lindholm, P.; Grönroos, T. J.; Forsback, S.; Sipilä, H.; Evans, S. M.; Solin, O.; Minn, H. ¹⁸F-EF5: A New PET Tracer for Imaging Hypoxia in Head and Neck Cancer. *J. Nucl. Med.* **2008**, *49*, 1944–1951.
- (54) Hendrickson, K.; Phillips, M.; Smith, W.; Peterson, L.; Krohn, K.; Rajendran, J. Hypoxia Imaging with [F-18] FMISO-PET in Head and Neck Cancer: Potential for Guiding Intensity Modulated Radiation Therapy in Overcoming Hypoxia-Induced Treatment Resistance. *Radiother. Oncol.* **2011**, *101*, 369–375.
- (55) Masaki, Y.; Shimizu, Y.; Yoshioka, T.; Tanaka, Y.; Nishijima, K.-i.; Zhao, S.; Higashino, K.; Sakamoto, S.; Numata, Y.; Yamaguchi, Y.; et al. The Accumulation Mechanism of the Hypoxia Imaging Probe "FMISO" by Imaging Mass Spectrometry: Possible Involvement of Low-Molecular Metabolites. *Sci. Rep.* **2015**, *5*, 16802.
- (56) Schwartz, J.; Grkovski, M.; Rimner, A.; Schöder, H.; Zanzonico, P. B.; Carlin, S. D.; Staton, K. D.; Humm, J. L.; Nehmeh, S. A. Pharmacokinetic Analysis of Dynamic ¹⁸F-Fluoromisonidazole PET Data in Non–Small Cell Lung Cancer. *J. Nucl. Med.* **2017**, *58*, 911–919.